THE JOURNAL OF PHYSICAL CHEMISTRY C
A JOURNAL OF THE AMERICAN CHEMICAL SOCIETY

pubs.acs.org/JPCC

Article

Strain-Induced Ferromagnetic to Antiferromagnetic Crossover in d^9-Ion (Cu^{2+} and Ag^{2+})-Layered Perovskites

Inés Sánchez-Movellán, Miguel Moreno, José Antonio Aramburu, and Pablo García-Fernández*

Cite This: *J. Phys. Chem. C* 2023, 127, 8332−8341

Read Online

ACCESS | Metrics & More | Article Recommendations | Supporting Information

ABSTRACT: A characteristic aspect of undoped high-temperature layered copper oxide superconductors is their strong in-plane antiferromagnetic coupling. This state is markedly different from that found in other chemically similar copper- or silver-layered fluorides, which display a ferromagnetic ground state. The latter has been connected in the literature with the presence of an orthorhombic deformation of the lattice that shifts the intermediate ligand between two metal ions to be closer to one and further from the other. This distortion is completely absent in the oxides, which are essentially tetragonal. However, no quantitative information exists about how this distortion influences the antiferromagnetic state and its relative stability with respect to the ferromagnetic state. Here, we carry out first-principles simulations to show that the fluorides in the parent tetragonal phase are also antiferromagnetic and that the antiferromagnetic-to-ferromagnetic transition is only triggered for a large enough distortion, with a typical ligand shift of 0.1 Å. Moreover, we employ a valence-bond model and second-principles simulations to show that the factor in superexchange that favors the antiferromagnetic state reduces as the ligand moves away from the symmetric metal−metal position. Importantly, we find that this distortion is sensitive to the application of an epitaxial strain which, in turn, allows controlling the difference of energy between ferromagnetic and antiferromagnetic states and thus the Curie or Néel temperatures. In fact, for compressive strains larger than 5.1%, this piezomagnetic effect makes K_2CuF_4 and Cs_2AgF_4 antiferromagnetic, making these two lattices close chemical analogs of oxide superconductors.

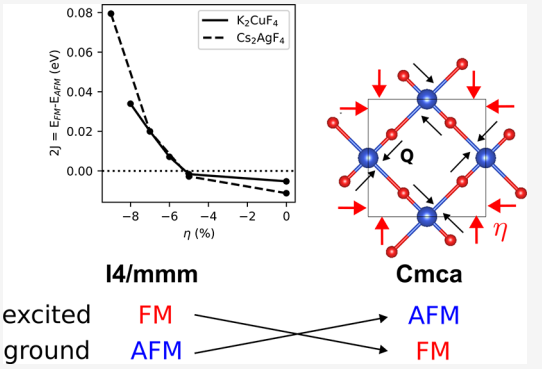

1. INTRODUCTION

Understanding the origin of high-T_C superconductivity in oxide cuprates is, arguably, one of the most important standing challenges in condensed matter physics.[1,2] Since its discovery[3] in hole-doped La_2CuO_4 in the late 80s, an enormous amount of research has been conducted in order to study the phenomenon from every possible point of view, but this extraordinary effort has raised many questions that, so far, have not been answered.[4−6] From the chemical point of view, it is surprising that high-T_C superconductivity is so specific to oxide cuprates with structures close to that of the layered perovskite La_2CuO_4, parent compound of the Ruddlesden−Popper A_2BX_4 family and is illustrated in Figure 1a. In these systems, layers of vertex-sharing six-coordinated B = Cu^{2+} ions are stacked and intercalated with connecting planes formed by the A cation that changes for the different high-T_C superconducting materials.[7−9] While the discovery of iron pnictides, whose structure also involves bidimensional transition-metal ion sheets, has clearly opened up the chemistry of compounds where high-T_C superconductivity is present, their differences with oxide cuprates are significant.[10] Thus, the question about whether it is possible to obtain lattices with an electronic structure that closely resembles that of the oxide cuprates without either copper or oxygen (or both) is still relevant.[11−14]

The search for these substitute high-T_C superconductors is constrained by the necessity to find an extremely specific system that not only has a layered structure but also displays a strong AFM ground state, typical of CuO_2 layers in La_2CuO_4. The search so far has not been successful as, for example, nickelates like $LaNiO_2$[14−16] contain Ni^+ ions that have a d^9 electronic structure like Cu^{2+} and are placed in bidimensional sheets, but the resulting magnetic coupling in the lattice is not AFM.

Other proposed compounds contain Ir or Rh[17,18] that have a spin S = 1/2 per metal ion, like Cu^{2+}, but, as yet, no superconductivity has been found. Perhaps, a more attractive possibility is to replace copper by silver which, being in the same group of the periodic table, is chemically similar. Moreover, instead of looking at oxides, it may be interesting to analyze the effect of replacing oxygen by fluorine as many

Received: February 20, 2023
Revised: April 17, 2023
Published: April 26, 2023

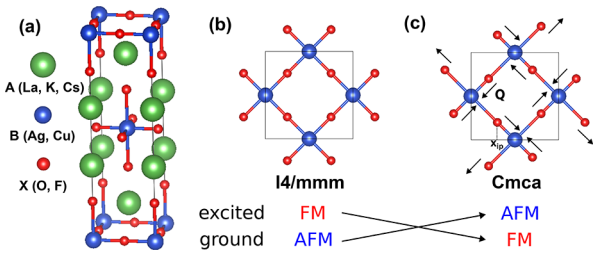

Figure 1. (a) Crystal structure of the A_2BX_4-layered perovskites. (b) Zenital view of one BF_2 (B = Cu and Ag) layer in the parent high-symmetry phase of K_2CuF_4 and K_2AgF_4, belonging to the tetragonal *I*4/*mmm* space group, with the antiferromagnetic (AFM) order in its ground state, while the ferromagnetic (FM) phase has higher energy. (c) Spontaneous antiferrodistortive (AFD) orthorhombic deformation taking place in the BF_2 layers of K_2CuF_4 and Cs_2AgF_4 giving rise to low-symmetry phases with an orthorhombic *Cmca* space group and FM ground state. The relationship between the distortion coordinate (Q) and the fractional position of in-plane fluorine ions (x_{ip}) is $Q = a(x_{ip} - 0.25)$, where a is the in-plane lattice constant.

perovskites containing this ion display comparable properties to those of the oxides. This has led to studying lattices like AgO that does not display magnetic ordering,[19] or AgF_2 that, despite some claims (see, e.g., refs 13 and 20), does not exhibit a layered structure.[21] The materials more closely resembling the La_2CuO_4 parent compound are K_2CuF_4 and Cs_2AgF_4. These three lattices are layered perovskites with the formula A_2BX_4, and the general structure is shown in Figure 1a. However, the structures are not completely alike since, in the oxide, the CuO_6 complexes are almost tetragonal but slightly tilted,[22] while in the two fluorides, the ligands in the metal plane undergo the AFD orthorhombic distortion as illustrated in Figure 1c. As discussed by Dai et al.[23] and Lee et al.,[24] the fact that La_2CuO_4 crystallizes[22] in an almost *I*4/*mmm* tetragonal structure (Figure 1b) and K_2CuF_4[25] and Cs_2AgF_4[26] in the orthorhombic *Cmca* one (Figure 1c) has a dramatic impact on the magnetism of the lattice as the oxide is AFM while in the fluorides it is FM, a change that prevents the appearance of superconductivity. However, and due to the similarity with La_2CuO_4, if the fluorides were to display an AFM state, they would become very interesting candidates for high-T_C superconductivity.

Due to the six-coordinated nature of the d^9 ions Cu^{2+} and Ag^{2+} in these lattices, the origin of the tetragonal distortion has often been associated to the Jahn–Teller (JT) effect.[27−30] However, the JT effect in isolated octahedral complexes never leads to an orthorhombic geometry[31] and, as we have extensively proven,[31−34] layered perovskites cannot be cubic, displaying, at most, a tetragonal symmetry that prevents in the case of d^9 ions the appearance of a parent high-symmetry phase with electronic degeneracy, the basic condition for the presence of the JT effect. In fact, a detailed study[34] of La_2CuO_4 compared with that of K_2CuF_4 showed that a key difference between the systems is that the gap between the two molecular orbitals of a tetragonal CuX_6 (X = O^{2-} and F^-) transforming like dz^2 and $dx^2 - y^2$ and coming from the σ-antibonding e_g level in a cubic crystal is controlled by the net charge of the AX (A = La^{3+} and K^+; X = O^{2-} and F^-) sheets with respect to that of the CuX_2 planes. In other words, the CuX_6 complexes are also subject to the electrostatic potential created by the rest of the lattice ions, which is quite different in La_2CuO_4 and K_2CuF_4.[34] In La_2CuO_4, this potential favors $dx^2 - y^2$ to be higher in energy, while in K_2CuF_4, dz^2 is the most energetic of the two, favoring, as a first step, a compressed configuration for the CuF_6 complex. As shown in ref 35, this compressed situation is particularly favorable for having an additional orthorhombic distortion in the layer plane that is helped by the simultaneous distortion of adjacent CuF_6 complexes sharing a common ligand. As discussed in Section 3.2, these factors are important to understand the magnetic coupling in these systems.

In the literature, there are studies that focus on the effect of the final geometry on the magnetic state.[23,24] There is also research on the origin of the distortion,[27−29] mostly concerned with the degeneracy of $dx^2 - y^2/dz^2$ orbitals. In this work, instead of focusing on the two static tetragonal and orthorhombic geometries as previous studies,[23,24] we examine, using first- and second-principles calculations, the mechanism by which the orthorhombic distortion induces the AFM to FM transition. A main goal of this work is to understand and quantify the mechanism by which the orthorhombic distortion induces the AFM to FM transition in layered perovskites, a key question that has not been adequately addressed in the literature. Interestingly, this study also allows us to find a strong piezomagnetic effect both in K_2CuF_4 and Cs_2AgF_4, which allows controlling the Curie or Néel temperature of both systems and triggers a crossover from an FM to an AFM ground state when a strong enough tensile epitaxial strain is in effect. This opens a new route to look for high-T_C superconductors in systems that closely match both the structure and magnetism of this family of compounds.

The paper is structured in the following manner: in Section 2, we provide the computational details for our first-principles simulations, while in Section 3, we present our results starting from the energy surfaces associated to the FM and AFM states with the orthorhombic distortion in Section 3.1. In Section 3.2, we discuss the mechanism of the distortion and different factors that affect each magnetic state when moving from the tetragonal to orthorhombic phase. Finally, in Section 3.3, we discuss the effect of epitaxial strain and how the crossover from the ground FM to AFM state can be produced. Conclusions are presented in Section 4.

2. METHODS

In order to show the strong dependence of the magnetic state with the structure of the system, we have carried out first-principles density functional theory (DFT) calculations using the CRYSTAL17 software suite.[36] Plain DFT functionals usually underestimate interelectronic interactions inside the strongly localized (internal) d-shell of transition metals. In solid-state problems, usual remedies involve the use of the semiempirical LDA + U method or hybrid DFT functionals. Here, we choose the later path to avoid introducing adjustable parameters in the simulation. In particular, we employ the PW1PW functional,[37] containing 20% Hartree–Fock exchange that, in combination with high-quality triple-ζ basis sets developed by Peintinger and co-workers,[38,39] has been shown to be able to accurately capture many subtle details of the structure of transition metal-containing crystals, for example, precise prediction of the octahedra rotation angle of many perovskites.[40]

The simulations are carried out in a $\sqrt{2} \times \sqrt{2} \times 1$ supercell that expands the *I*4/*mmm* conventional cell of the aristotype compound, K_2NiF_4, in order to accommodate the both in-plane FM and AFM states and symmetry-lowering AFD distortions to the *Cmca* group. Integration on the first Brillouin

https://doi.org/10.1021/acs.jpcc.3c01166
J. Phys. Chem. C 2023, 127, 8332−8341

Table 1. Summary of Results of DFT Optimization Calculations for Unstrained K_2CuF_4 and Cs_2AgF_4[a]

system	state	phase	a (Å)	b (Å)	c (Å)	x_{ip}	ΔE/formula (meV)
K_2CuF_4	FM	$I4/mmm$	5.875	5.875	12.645	0.2500	4.5
		$Cmca$	5.865	5.864	12.760	0.2696	−105.5
			5.866	***5.866***	***12.734***	***0.2670***	
	AFM	$I4/mmm$	5.876	5.876	12.637	0.2500	0.0
		$Cmca$	5.866	5.866	12.761	0.2700	−100.1
Cs_2AgF_4	FM	$I4/mmm$	6.485	6.485	14.244	0.2500	7.9
		$Cmca$	6.454	6.455	14.382	0.2693	−126.3
			6.434	***6.439***	***14.149***	***0.2681***	
	AFM	$I4/mmm$	6.484	6.484	14.238	0.25	0.0
		$Cmca$	6.461	6.461	14.371	0.2697	−114.6

[a]Lattice parameters a, b, and c, the atomic position of the in-plane fluorine ligands, x_{ip}, and the energy difference between states is provided. The energy reference is taken as the ground state high-symmetry configuration (tetragonal AFM phase). Experimental lattice parameters are indicated in bold font (extracted from refs 25 and 26 for K_2CuF_4 and Cs_2AgF_4, respectively).

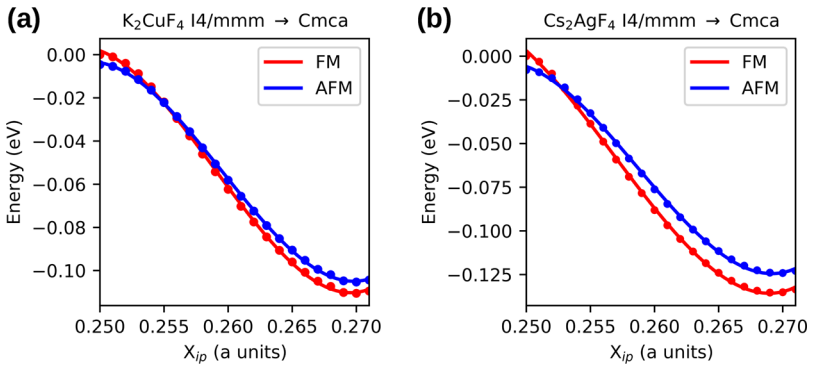

Figure 2. Energy surfaces of (a) K_2CuF_4 and (b) Cs_2AgF_4 at zero strain. The energy (given per formula unit) has been obtained by single point calculations throughout the AFD distortion from the parent tetragonal $I4/mmm$ phase to the minimum at the orthorhombic $Cmca$ one.

zone was performed with the use of an 8 × 8 × 4 grid, which gives a spacing of 0.133, 0.133, and 0.123 $Å^{-1}$ between each **k** point of the reciprocal space, while real-space integrals of the electron density were obtained with an extralarge grid and the various truncation criteria for bielectronic integrals (ITOL1 to ITOL5) were set to 9, 9, 9, 9, and 18. The total energies were converged below 10^{-9} hartree.

In order to study the dependence of the magnetic coupling in these systems on various details of the electronic structure (metal and ligand level positions, metal−ligand hopping parameters, intra-atomic electron repulsion, and metal−ligand force constant), we have built a reduced second-principles model for these lattices. It reproduces a 2D MX_2 plane (M = Cu and Ag) that contains Wannier functions representing dz^2, $dx^2 - y^2$ metal functions and σ-bonding p-functions on the ligands. The model was then trained to reproduce the bands obtained from DFT simulations for FM and AFM states. Total energies obtained from this model (which are not included in the training) reproduce DFT results with good accuracy.

3. RESULTS

3.1. Nonstrained Ground State. Results of the DFT geometry optimizations carried out for unstrained K_2CuF_4 and Cs_2AgF_4 systems are shown in Table 1 for both the parent high-symmetry (tetragonal $I4/mmm$) and low-symmetry (orthorhombic $Cmca$) critical points of the energy surface, with the relative stability of the FM and AFM phases in each structure. We can see that, in full agreement with low temperature experimental characterization, our simulations find that the lowest energy configuration for these systems involves the AFD orthorhombic deformation ($x_{ip} \neq 0.25$), as illustrated in Figure 1c. In fact, comparing the cell parameters and metal−ligand distances obtained in simulations with X-ray diffraction data,[25,26] we see that our simulations involve small errors below 2% in interatomic distances.

From the data in Table 1, it is clear that the FM phase is below the AFM one when the lattice is distorted ($Cmca$ group), in agreement with experimental data,[25,26] while the order of the states is reversed at the parent high-symmetry geometry ($I4/mmm$). However, the energy difference is always small, remaining in the 1−10 meV range. This important result means that the order of the states is sensitive to the geometry and that there exists a crossover from an AFM phase to an FM one as the system distorts. It is notable that even though the orthorhombic distortion is completely localized on MX_2 planes, the a and b lattice parameters are not strongly affected by it, increasing by less than 1% when going from the tetragonal phase to the orthorhombic one. While this seems to indicate that the energy is largely insensitive to the in-plane lattice constant, we will later see that this is not the case, as these materials display a large piezomagnetic effect. We can also see in Table 1 that for both K_2CuF_4 and Cs_2AgF_4 systems, the absolute value of the energy difference between the FM and AFM phases, $\delta = E_{FM} - E_{AFM}$, is similar for the high- and low-symmetry configurations in both systems (but the sign of δ is opposite), although it is larger in the argentate ($\delta \approx 10$ meV) than in the cuprate ($\delta \approx 5$ meV).

Another important conclusion that can be extracted from Table 1, and not discussed in the literature,[23,24,27−29] is that the orthorhombic distortion is present in both FM and AFM

https://doi.org/10.1021/acs.jpcc.3c01166
J. Phys. Chem. C 2023, 127, 8332−8341

states. This key factor can be clearly observed in Figure 2, where we have fixed the lattice parameters of the system and plotted the energy of the FM and AFM states as the orthorhombic AFD was followed. We can see that in both K_2CuF_4 and Cs_2AgF_4, the FM and AFM states at the $I4/mmm$ phase are unstable with respect to the AFD distortion, presenting at this point a local maximum in the energy surface. However, the instability of the tetragonal $I4/mmm$ phase is weaker in the AFM state than in the one corresponding to the FM state. This can be clearly seen in the stabilization energy associated with the distortion, defined as the reduction in energy of the system in each state when distorted along the AFD motion, $\Delta E_Q = E_{ORT} - E_{TET}$. In the case of the cuprate, the stabilization energy is $\Delta E_Q = -110$ and -100 meV for the FM and AFM phases, respectively, while for the argentate, these values are slightly larger, -130 and -110 meV. Thus, we can observe in Figure 2 that in both systems, the AFM state has a stabilization energy that is only around 20 meV smaller than the one corresponding to the FM configuration. Furthermore, it should be stressed that as the distortion is realized, there is a crossing between the energy curves of the AFM and FM states, the latter becoming the ground state. The crossover point is quite close to the high-symmetry point in Cs_2AgF_4 and somewhat closer to the minimum in K_2CuF_4 (see Figure 2). These results are intriguing and open up the question of how far the system can be tuned with respect to parameters like δ that controls the Curie or Néel temperature in these materials, or how sensitive to external perturbations, like strain, the instability in each of the states is. In the following study, we will analyze in detail the electronic structure of these materials in order to find the chemical mechanisms behind the magnetic changes created by the distortion in these systems and the insights they provide will be used to manipulate the relative energies of these states.

3.2. Electronic Structure of Layered d^9 Perovskites. In order to understand the change in electronic and magnetic structures with the orthorhombic distortion, we will use two approaches. First, we will develop a qualitative model based on valence-bond theory that provides a simple explanation for both the instability of the FM and AFM states and their relative stability with the orthorhombic distortion. Then, we will build a semiquantitative second-principles model[41] to understand the variation of the total energy of the system with the distortion that will help us predict its behavior when epitaxial strain is applied.

Valence-bond models have been widely used to describe magnetism,[42,43] the well-known Anderson's superexchange model[44,45] being the canon, which he also used to describe a possible mechanism for high-T_C superconductivity in La_2CuO_4.[46] In order to describe in a natural way the effects of the AFD distortion on the magnetism of K_2CuF_4 and Cs_2AgF_4, we have constructed a valence-bond model somewhat different from Anderson's, as to the starting point and the excitations considered, but its qualitative results for the undistorted systems are the same. In a similar way to the model proposed by Solomon and co-workers in refs 47 and 48, the present model describes the ligand's orbitals, explicitly allowing us the introduction of the vibronic coupling responsible for the distortion in a simple manner.

Our starting point is a system of two metal ions containing one active magnetic orbital each (dz^2 in the fluorides and $dx^2 - y^2$ in the oxides, see ref 34) and a σ-bonding p-function localized on a bridging ligand (see Figure 3). Considering that the metal orbitals are spatially separated, their interactions need to be mediated by the ligand, which forms a single bond with each of the metals.

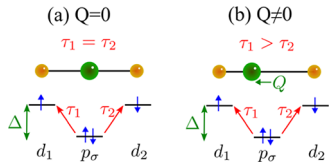

Figure 3. Scheme of the orbitals, metal−ligand splitting, Δ, and hopping parameters, τ_i, used in the valence-bond model for (a) undistorted symmetric structure ($Q = 0$), where $\tau_1 = \tau_2$, and (b) asymmetric complex ($Q \neq 0$), where the ligand is closer to the metal ion 1 and $\tau_1 > \tau_2$.

Using perturbation theory (see the Supporting Information for the detailed description of the model), we find that the energies for the FM and AFM states are, respectively

$$E_{FM} \approx E_0 - [\tau_1^2/(\Delta + U - K) + \tau_2^2/(\Delta + U - K)] \quad (1)$$

$$E_{AFM} \approx E_0 - [\tau_1^2/(\Delta + U) + \tau_2^2/(\Delta + U) + 2\tau_1^2\tau_2^2/(\Delta + U)^3] \quad (2)$$

where E_0 is the energy of the ground configuration for both FM and AFM states, Δ is the one-electron energy difference between the metal and ligand levels (see Figure 3), U is the penalty energy associated to adding an extra electron to a metal atom, K is the small exchange integral between metal and ligand orbitals, and τ_1 and τ_2 are the hopping matrices (in the tight-binding sense[49]) from the ligand orbital to the orbitals localized on the first and second metal atoms, respectively. The first two terms inside the parenthesis in eqs 1 and 2 represent the energy of each of the individual metal−ligand bonds in the metal−ligand−metal complex, as indicated by the hopping matrix elements τ_1 and τ_2.

Let us first consider the symmetric situation in which the $M^{2+}-F^--M^{2+}$ dimer (M = Cu and Ag) has an inversion center, with $\tau_1 = \tau_2 = \tau_0$ (Figure 3). Considering only the first two terms inside the parentheses in eqs 1 and 2, it can be seen that the energy for the FM state, E_{FM}, would be a little lower than the AFM one, E_{AFM}, due to the small metal−ligand direct exchange interaction K. However, the AFM energy contains a third term that depends on $\tau_1^2\tau_2^2$, involving a simultaneous electron excitation from the ligand to each of the surrounding metal ions, that is, it has a collective character affecting both bonds at the same time. From the above, if we consider that the effect of K is small, AFM states will be stabilized with respect to FM ones due to this extra term in eq 2. This is consistent with Anderson's model where direct exchange favors the FM coupling while a large hopping integral, τ_i, lowers the energy of the AFM state. Moreover, given that the term favoring the AFM state in the symmetric dimer is proportional to τ_0^4, its effect is strongly dependent on the magnitude of the hopping, which is much larger in oxides, since it would be roughly proportional to the overlap of the $dx^2 - y^2$ function, lying in the layer plane, with a ligand function in the same plane, than in fluorides, where the metal function has a dominant dz^2 character, being thus perpendicular to the plane.

Now, we consider the effects of a small orthorhombic distortion (Figures 1c and 3b), with the coordinate $Q \approx (x_{ip} -$

https://doi.org/10.1021/acs.jpcc.3c01166
J. Phys. Chem. C 2023, 127, 8332−8341

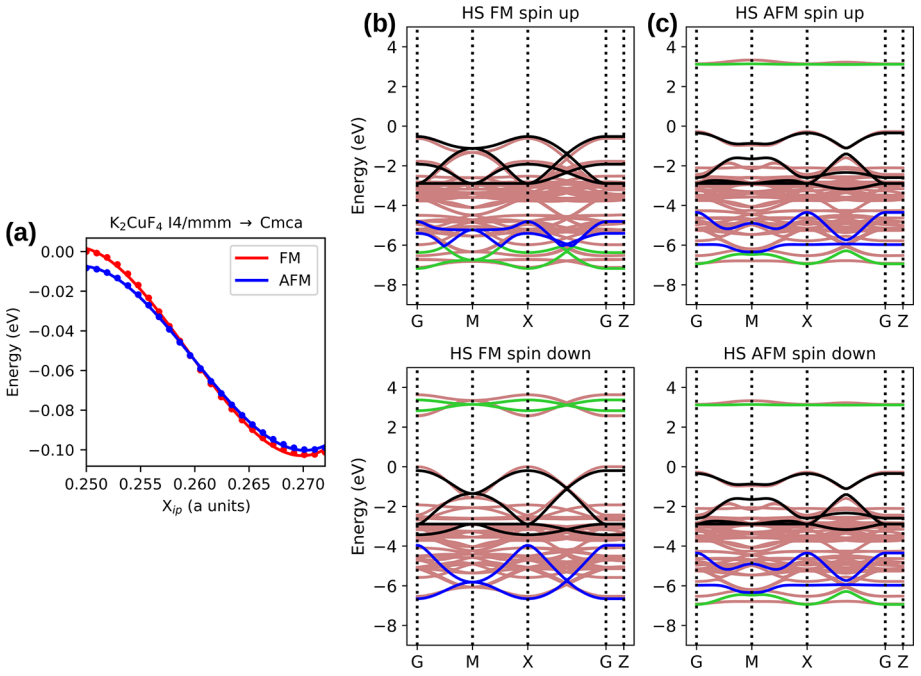

Figure 4. Results of the second-principles simulations for K_2CuF_4. (a) Variation of the total energy with the AFD distortion. (b) Band structure of the FM phase of the high-symmetry (HS) *I4/mmm* phase ($Q = 0$ in (a)). The upper and bottom panels represent the spin-up and spin-down bands, respectively. (c) Idem, for the AFM phase. The bands obtained from first-principles calculations are represented in dark salmon color, while the bands calculated from second-principles are distinguished by their main contribution: bands coming from the Cu^{2+} ions are displayed in green (mainly $3z^2 - r^2$ characters) and blue ($\sim x^2 - y^2$) whereas the black ones represent p_σ orbitals of F^- ligands.

$0.25)a$ ($|Q| \ll 0.25a$), leading to a nonsymmetric dimer. Then, τ_1 and τ_2 can be written as

$$\tau_1 = \tau_0 + fQ + O(Q^2) \tag{3}$$

$$\tau_2 = \tau_0 - fQ + O(Q^2) \tag{4}$$

where f is the linear vibronic coupling constant[27] that measures the change of the hopping integral with the variation of the metal−ligand distance, and the ± sign accounts for the increase/decrease of τ_i when the metal−ligand distance becomes larger/smaller, respectively. Then, using eqs 1−4 we find

$$E_{FM} \approx E_0 - 2(\tau_0^2 + f^2Q^2)/(\Delta + U - K) \tag{5}$$

$$E_{AFM} \approx E_0 - 2(\tau_0^2 + f^2Q^2)/(\Delta + U) - 2(\tau_0^4 - 4\tau_0^2 f^2 Q^2)/(\Delta + U)^3 \tag{6}$$

As in eqs 1 and 2 above, the second term in eqs 5 and 6 corresponds to the sum of the energy of the individual bonds, while the third term in eq 6 corresponds to the collective excitation of both electrons in the ligand toward the metals. In the absence of orthorhombic distortion ($Q = 0$), the term in τ_0^4, arising from the collective excitation, favors the AFM configuration. By contrast, the absolute value of this term decreases with the distortion, triggering the AFM to FM crossover. A key result is that, if the bond with the metal 2 is destroyed by the distortion, then $\tau_2 = 0$ and the key term favoring the AFM phase in eq 2 becomes zero as it depends on $\tau_1^2\tau_2^2$. Obviously, the distortion modifies the covalency between the ligand and the two metal ions, something that is fully supported in our DFT simulations (see Figure S4 in the Supporting Information). The main conclusion that can be extracted from the model is that a reduction in the orthorhombic distortion could allow these d^9 fluorides to revert into an AFM state similar to that of La_2CuO_4 and other high-temperature cuprate oxides.

While the model above qualitatively describes the relative stability of the FM and AFM states, it cannot be used to calculate the total energy of the system. A simple approach that could allow us to perform this task is the second-principles parameterization of the system. Second-principles DFT[41] is an approach to carry out large-scale simulations in condensed matter using a force field and a tight-binding-like description of the bands that include both electron−lattice and electron−electron interactions. While a full parameterization of the layered perovskites under study could provide a fully quantitative description of the bands and energy surfaces of the system, here we will aim for a minimal model that expands on the ideas exposed above and allows us to understand how to manipulate magnetism in the studied layered fluorides.

First, we consider that the magnetic states are strongly confined within the BX_2 layers (see Figure 1) and that the influence of the A cations in the lattice can be reduced to a purely electrostatic effect. Indeed, in Figure 4, one can observe that the dispersion of the valence bands along the z-direction is small, indicating that the ligand-p and metal-d orbitals are rather confined within the atomic sheets accommodating the d^9-ions. This has a strong influence on the properties of these systems as, for example, the weak magnetic coupling between layers has been proposed to come from magnetic dipolar interactions.[50] Thus, we focus on determining the electronic structure on the two-dimensional BX_2 layers where the distortion of the system is also contained. The model consists of a harmonic potential to account for the stiffness of the in-plane metal−ligand bond and a geometry-dependent tight-bonding model enhanced with electron−electron interactions within the d^9-ion orbitals to take into consideration the band

https://doi.org/10.1021/acs.jpcc.3c01166
J. Phys. Chem. C 2023, 127, 8332−8341

structure and magnetic interactions. The basis for the tight-binding model (see Figure 3) is mainly the $dx^2 - y^2$ and dz^2 (Wannier-like) localized functions on the transition metal and the p_σ orbitals mainly localized over the ligands. We consider the Slater–Koster matrix elements[49] between each of the metal orbitals with the p_σ levels of the neighboring ligands. Moreover, we consider that these interactions depend on the metal–ligand distance linearly, as allowed by the symmetry of the system, and expressed above in eqs 3 and 4. Intra-atomic electron–electron interactions within the manifold of $dx^2 - y^2$ and dz^2 orbitals are modeled within the Hartree–Fock theory, assuming the shape of the orbitals responds, approximately, to spherical symmetry, following the ligand-field theory[51] or LDA + U.[52] As in the latter approach, we will use Hubbard and exchange parameters to describe intra-atomic electron–electron interactions. All parameters describing K_2CuF_4 and Cs_2AgF_4 are given in Table 1 of the Supporting Information.

Main results of the second-principles simulations for K_2CuF_4 are shown in Figure 4, including the fitted FM and AFM bands at the high- and low-symmetry phases and predicted energy surfaces by the models. We can see that even though the model simplifies the complex electronic structure of these systems to a minimum, i.e., it does not contain many of the orbitals of the system, it still captures many of the key features of the band diagram, like the dispersion of the d-bands for each of the magnetic states. Moreover, the dependence of the energy on the distortion in Figure 4 presents a strong similarity to the DFT ones (Figure 2) displaying a saddle point at $x = 0$ with an AFM ground state and a crossover to an FM ground state when moving toward the $x \neq 0$ minimum as well as similar stabilization energies for both magnetic states. Thus, we consider our second-principles modeling an adequate starting point to study how to manipulate these fluorides to achieve an AFM ground state like in cuprate oxides.

With regard to building models for these layered perovskites, it is important to note that the bands cannot be properly reproduced if the diagonal Hamiltonian element of the Wannier-like $dx^2 - y^2$ and dz^2 orbitals is taken to be the same. This fact is clearly supported by symmetry since the Wyckoff position for the metal site in layered perovskites has tetragonal symmetry, which leads the $dx^2 - y^2$ and dz^2 levels to be nondegenerate. The splitting between these levels, given in our tight-binding parameters, is significant (approximately 3.2/1.8 eV in K_2CuF_4 and Cs_2AgF_4, respectively) and clearly shows that JT or Kugel–Khomskii models,[27−29] usually applied to explain the properties of these systems, are not valid as they are based on the degeneracy of these levels. In particular, the Kugel–Khomskii model for these systems[28,29] predicts that the FM state will be the ground state in the high-symmetry configuration, which is clearly wrong according to our DFT simulations. The correct framework to describe the distortion in these systems is the vibronic coupling given by the pseudo Jahn–Teller (PJT) effect,[27] whose chemical interpretation is quite different from the JT effect, despite the fact that their names would seem to suggest otherwise. Within this approach the total force constant K_T at the high-symmetry geometry is the sum of two contributions

$$K_T = K_0 + K_v \tag{7}$$

Here, K_0 is the elastic nonvibronic contribution to the force constant, which is positive[27] and represents the resistance of the bonds to be deformed from the high-symmetry configuration. In the model (eqs 1 and 2) this corresponds with

$$K_0 = d^2E_0/dQ^2 \tag{8}$$

while K_v is the vibronic contribution to the force constant

$$K_v = -f^2/(E_e - E_g) \tag{9}$$

which is negative since the difference between the excited state energy (E_e) and the ground state (E_g) energy is positive and represents the creation of new bonding mechanisms when symmetry restrictions on the wavefunctions are lifted by the distortion. A spontaneous symmetry-breaking instability is activated when $|K_v| > K_0$ and so $K_T < 0$ helping to stabilize the lower-symmetry geometry. This phenomenon, both in the PJT model and in our bond-valence and second-principles models, is accounted for by the orbital vibronic constant f that measures how the metal–ligand Hamiltonian elements change with the metal–ligand distance. Here, we can now inspect eqs 5 and 6 to find that the terms proportional to Q^2 are indeed negative, thus indicating that they help to stabilize the geometries with $Q \neq 0$ both for the FM and AFM states. However, the predicted vibronic contributions to the force constant for the FM and AFM states are different

$$K_v(\mathrm{FM}) = -f^2/(\Delta + U - K) \tag{10}$$

$$K_v(\mathrm{AFM}) = -f^2/(\Delta + U) + 2\tau_0{}^2f^2/(\Delta + U)^3 \tag{11}$$

From the above expressions, the force constant for the FM state is necessarily more negative than that for the AFM, a fact in full agreement with our DFT simulations. The reasons that follow from the discussion above and are consistent with results from Anderson's model are twofold:

(i) Excited states for the FM state are somewhat lower in energy than for the AFM state, as reflected in the denominator of eqs 10 and 11.

(ii) The effect of the vibronic coupling is somewhat smaller in the AFM state, as reflected by the second term in eq 11, representing that the bonding in this state has a greater preference for high symmetry than its FM counterpart.

Moreover, we would like to remark that the models presented here stress the importance of the coupling between the metal and ligand levels, which contrast with usual JT-like models where the coupling occurs between dz^2 and $dx^2 - y^2$ orbitals. While it is true that coupling with both metal orbitals reinforces this distortion, the initial tetragonal symmetry of the system and the significant splitting of these levels controls the physical behavior of these systems and sets it quite far apart from what happens in systems with degeneracy. Thus, as we found in other systems with similar orthorhombic distortion, our models indicate that the low initial symmetry, preventing degeneracy, underscores the importance of metal–ligand PJT coupling.

From the discussion above, we can conclude that a large distortion will favor the appearance of an FM state. In particular, the energy difference between FM and AFM states is

$$2J = E_{FM} - E_{AFM} = \Delta E(Q = 0) - \alpha Q^2 \tag{12}$$

where

$$\alpha = 2f^2K/(\Delta + U)^2 + 8\tau_0{}^2f^2/(\Delta + U)^3 \tag{13}$$

https://doi.org/10.1021/acs.jpcc.3c01166
J. Phys. Chem. C 2023, 127, 8332−8341

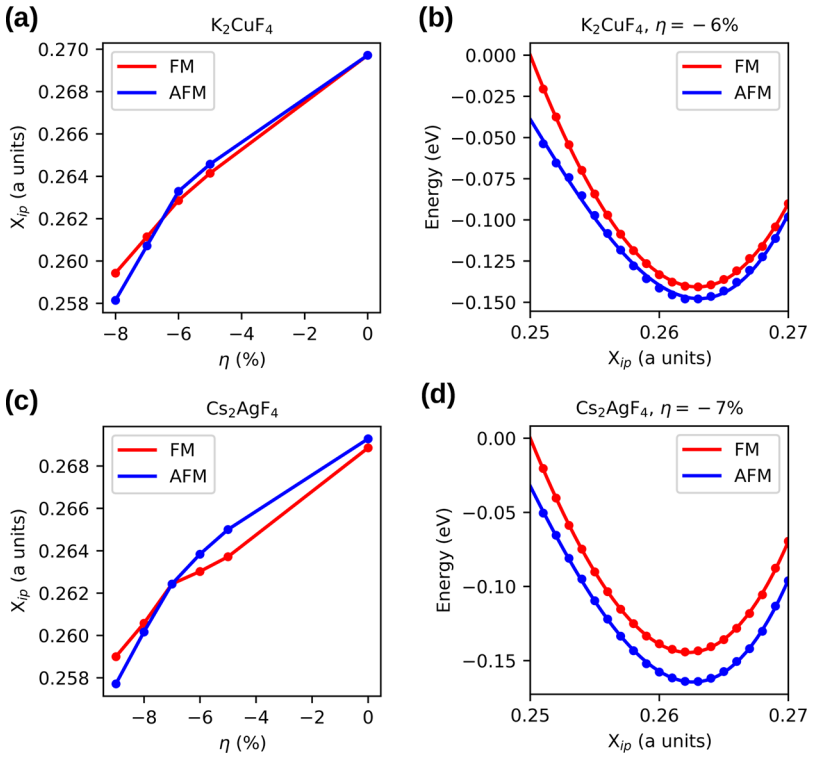

Figure 5. Evolution of the equilibrium position in the distortion (x_{ip}) with strain η for FM and AFM phases of (a) K_2CuF_4 and (c) Cs_2AgF_4. The energy surfaces when a sufficient strain (η = −7.1 and −7.4% for K_2CuF_4 and Cs_2AgF_4, respectively) is applied to prevent the AFM to FM crossover are shown in (b) and (d).

$$\Delta E(Q=0) = -2\tau_0^2 K/(\Delta + U)^2 + 2\tau_0^4/(\Delta + U)^3 \quad (14)$$

favoring an FM coupling with increasing Q.

However, the above expressions do not allow prediction of the position of the minima in the energy surface of the system. This is the point where the second-principles modeling is quite useful. In order to obtain the absolute position of the minima and the relative energy between the FM and AFM states, it is necessary to consider the effect of K_0 in eq 7, which is given by the base harmonic force constant of the metal−ligand bond in the second-principles model. Our calculations show that a weak metal−ligand force constant K_0 leads to large distortions and allows the FM−AFM crossover. However, as the metal−ligand force constant becomes stronger, the crossover occurs closer to Q = 0 until a large enough K_0 value where it disappears, and the global minimum of the system becomes AFM as indicated by eq 12.

While the vibronic contribution K_v is directly associated to the electronic structure of the system and is difficult to manipulate, the force constant K_0 is associated to the in-plane metal−ligand distances represented in Figure 1b,c. These distances can be controlled by applying to the system an epitaxial strain

$$\eta = (a^* - a)/a \quad (15)$$

and thus controlling the position of the minimum and the relative stability of the FM and AFM phases. In the equation above, a^* represents the in-plane lattice parameter when the strain is non-null. This effect is further reinforced by the fact that $\Delta E(Q=0)$ (eq 14) increases with τ_0 which, in turn, grows when the metal−ligand distance is reduced (η < 0).

3.3. Effect of an Epitaxial Strain. Epitaxial engineering is a particularly important topic in perovskite materials and has been used, for example, to manipulate magnetism to obtain a ferroelectric-FM system[53] or alter the polar states in PbTiO3/SrTiO3 superlattices from a vortex lattice when grown in $DyScO_3$[54] to a skyrmion lattice when grown on SrTiO3.[55] In other systems,[56−58] including perovskites,[58] application of strain has been shown to be an effective way to change the magnetic state of a system. We can simulate the effect of epitaxial strain in our DFT simulations by fixing the in-plane lattice parameter and relaxing the rest of the structure.

The calculations respond in the way expected from the discussion in Section 3.2. Upon increasing the lattice parameter (η > 0), the distortion at equilibrium represented by the x_{ip} parameter grows both for the FM and AFM states. At the same time the stabilization energy for both states increases, although it does it at a faster rate for the FM state. When the lattice parameter is decreased (η < 0, see Figure 5a,c), the distortion becomes smaller and the FM−AFM energy difference reduces until the crossover disappears at η = −5.3% for both K_2CuF_4 and Cs_2AgF_4 (see Figure 6). Typical energy surfaces for this situation are shown in Figure 5b,d. In both cases, it is found that the ground state of the system becomes AFM in an analogous situation to what is found in cuprate oxide superconductors. As can be observed in Figure 5, the equilibrium position in both K_2CuF_4 and Cs_2AgF_4 is significantly smaller than that at η = 0 and in agreement with our models.

Thus, our simulations show the presence of a strong piezomagnetic effect[56−58] in fluoride perovskites that can be used to tune the energy difference between the FM and AFM states, controlling the magnetic transition temperatures and even allowing the system to crossover from FM to AFM when

https://doi.org/10.1021/acs.jpcc.3c01166
J. Phys. Chem. C 2023, 127, 8332−8341

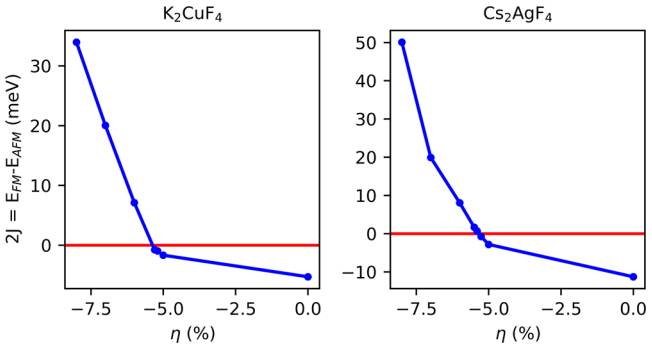

Figure 6. Change of the effective magnetic coupling constant $2J = E_{FM} - E_{AFM}$ with strain. The curves for K_2CuF_4 and Cs_2AgF_4 are, respectively, shown in the left and right panels.

a strong enough tensile stress is applied. These results are summarized in Figure 6 where the energy difference $E_{FM} - E_{AFM}$ is plotted against the strain. Not only that but Figure 3 shows that these systems display a significant piezomagnetic effect that can be used to tune the effective magnetic coupling constant $J = (E_{FM} - E_{AFM})/2$ that provides with a measure of the Curie or Néel temperatures above and below the strain for the FM to AFM crossover. The fact that an increase in the metal−ligand distance reduces the AFM coupling is fully consistent with the experimental trends found in cubic Ni^{2+} and Mn^{2+} fluorite perovskites[59] where the application of pressure and the associated reduction of the metal−ligand distance increased the absolute value of the effective coupling constant, J, thus enhancing the stability of the AFM state. Moreover, our calculations show that while for strains above the crossover ($\eta \approx -5\%$) the piezomagnetic effect is moderate, below this threshold, the variation of the coupling constant J with stress is strongly nonlinear, particularly in the case of the argentate. This is consistent with the fact that covalency in the silver−fluorine bond is stronger than the copper−fluorine one, making τ_0 larger in the argentates.[60] Grochala and others[12,13] have tried to exploit this property to obtain strongly AFM argentate lattices.

4. CONCLUSIONS

In this paper, we have described the chemical mechanisms that control the stability of the FM state with respect to the AFM one in the high-T_C oxide cuprate analogs K_2CuF_4 and Cs_2AgF_4. Our main result is that we have found, for the first time, that an AFM ground state in these fluorides is possible under conditions of tensile epitaxial strain, although we assume a similar effect can be obtained by other means like, for example, replacing, partially, K^+ ions by Na^+ in K_2CuF_4, although it must be noted that Na_2CuF_4 displays a different crystalline structure. This kind of ground state is one of the most important characteristics of undoped La_2CuO_4, the parent compound of high-temperature superconductors. Furthermore, we have provided detailed quantitative and qualitative models of the relative stability of the FM and AFM states and their evolution with the orthorhombic distortion characteristic of these fluorides. These models show how, while both states display the AFD orthorhombic instability, a small increase of covalency, associated to the simultaneous transfer of two of the ligands' electrons to the metals, favors the AFM coupling at small distortions while at deformations larger than $Q = 0.1$ Å, the studied systems prefer the FM phase. As these energy differences are quite sensitive to the in-plane lattice constant, we conclude that stress can be used to tune the Curie/Neél temperatures (respectively, for FM/AFM regimes), showing the presence of a significant piezomagnetic effect in these systems.

Concluding, we would like to note that some highly relevant models for high-T_C superconductivity (most notably ref 46) rely, essentially, on a strong superexchange interaction to support the AFM state and this has pushed the community to look for similar systems with related characteristics (see, e.g., ref 12). The present work provides some new ideas to test these foundations, but we believe some caution is necessary. Even though we propose a mechanism to control the magnetic transition energies and revert their signs, experimentally these energies are found to be invariably small (below 10 K) in d^9-layered fluorides and we expect that this trend will not change significantly with the application of strain. This energy scale contrasts with the one find in cuprates where the order changes at higher temperatures (around 275 K) and this points toward some other fundamental factors in their physics, like the nature of the unpaired electrons (dz^2 in fluorides vs $dx^2 - y^2$ in cuprates) that can be associated to the charge of the layers that form the lattice[34] and which is distinct from the mechanism discussed above. We hope that these new insights into the structure of these interesting systems can provide some insights into the high-T_C superconductor puzzle. Further research on the correlation of superexchange and structure in these lattices is underway.

■ ASSOCIATED CONTENT

Supporting Information

The Supporting Information is available free of charge at https://pubs.acs.org/doi/10.1021/acs.jpcc.3c01166.

Details on the expressions used for the valence-bond model and the detailed diagrams of the one-electron density (PDF)

■ AUTHOR INFORMATION

Corresponding Author

Pablo García-Fernández − *Departamento de Ciencias de la Tierra y Física de la Materia Condensada, Universidad de Cantabria, 39005 Santander, Spain;* orcid.org/0000-0002-4901-0811; Email: garciapa@unican.es

Authors

Inés Sánchez-Movellán − *Departamento de Ciencias de la Tierra y Física de la Materia Condensada, Universidad de Cantabria, 39005 Santander, Spain*

Miguel Moreno − *Departamento de Ciencias de la Tierra y Física de la Materia Condensada, Universidad de Cantabria, 39005 Santander, Spain*

José Antonio Aramburu − *Departamento de Ciencias de la Tierra y Física de la Materia Condensada, Universidad de Cantabria, 39005 Santander, Spain;* orcid.org/0000-0002-5030-725X

Complete contact information is available at: https://pubs.acs.org/10.1021/acs.jpcc.3c01166

Notes

The authors declare no competing financial interest.

https://doi.org/10.1021/acs.jpcc.3c01166
J. Phys. Chem. C 2023, 127, 8332−8341

■ ACKNOWLEDGMENTS

We acknowledge financial support from Grant No. PGC2018-096955-B-C41 funded by MCIN/AEI/10.13039/501100011033. I.S.M. acknowledges financial support from grant BDNS:589170 (Gobierno de Cantabria-Universidad de Cantabria).

■ REFERENCES

(1) Anderson, P. W.; Lee, P. A.; Randeria, M.; Rice, T. M.; Trivedi, N.; Zhang, F. C. The physics behind high-temperature superconducting cuprates: the 'plain vanilla' version of RVB. *J. Phys.: Condens. Matter* **2004**, *16*, R755−R769.

(2) Tsymbal, E. Y.; Dowben, P. A. Grand challenges in condensed mater physics: from knowledge to innovation Front. *Front. Phys.* **2013**, *1*, 32.

(3) Bednorz, J. G.; Müller, K. A. Possible high Tc superconductivity in the Ba-La-Cu-O system Z. *Phys. B* **1986**, *64*, 189−193.

(4) O'Mahony, S. M.; Ren, W.; Chen, W.; Chong, Y. X.; Eisaki, H.; Uchida, S.; Hamidian, M. H.; Davis, J. C. S. On the electron paring mechanism of copper-oxide high temperature superconductivity. *Proc. Natl. Acad. Sci. U. S. A.* **2022**, *119*, No. e2207449119.

(5) Kowalski, N.; Dash, S. S.; Sémon, P.; Sénéchal, D.; Tremblay, A. M. Oxygen hole content, charge-transfer gap, covalency and cuprate superconductivity. *Proc. Natl. Acad. Sci. U. S. A.* **2021**, *40*, No. e2106476118.

(6) Li, H.; Zhou, X.; Parham, S.; Reber, T. J.; Berger, H. M.; Arnold, G. B.; Dessau, D. S. Coherent organization of electronic correlations as a mechanism to enhance and stabilize high-Tc cuprate superconductivity. *Nat. Commun.* **2018**, *9*, 26.

(7) Wu, M. K.; Ashburn, J. R.; Torng, C. J.; Hor, P. H.; Meng, R. L.; Gao, L.; Huang, Z. J.; Wang, Y. Q.; Chu, C. W. *Superconductivity at 93 K in a New Mixed-Phase Y-Ba-Cu-O Compound System at Ambient Pressure", Ten Years of Superconductivity: 1980−1990, Perspectives in Condensed Matter Physics*; Springer Netherlands: Dordrecht, 1993; Vol. 7; pp 281−283

(8) Sheng, Z. Z.; Hermann, A. M. Bulk superconductivity at 120 K in the Tl−Ca/Ba−Cu−O system. *Nature* **1988**, *332*, 138−139.

(9) Schilling, A.; Cantoni, M.; Guo, J. D.; Ott, H. R. Superconductivity above 130 K in the Hg−Ba−Ca−Cu−O system. *Nature* **1993**, *363*, 56−58.

(10) Si, Q.; Yu, R.; Abrahams, E. High-Temperature superconductivity in iron pnictides and chalcogenides. *Nat. Rev. Mater.* **2016**, *1*, 16017.

(11) Yang, X.; Su, H. Cuprate-like electronic properties in superlattices with AgF_2 square sheet. *Sci. Rep.* **2014**, *4*, No. 05420.

(12) Grochala, W. Silverland: the Realm of Compounds of Divalent Silver − and why they are interesting. *J. Supercond. Novel Magn.* **2018**, *31*, 737−752.

(13) Gawraczyński, J.; Kurzydlowski, D.; Ewings, R. A.; Bandaru, S.; Gadomski, W.; Mazej, Z.; Ruani, G.; Bergenti, I.; Jaroń, T.; Ozarowski, A.; et al. Silver route to cuprate analogs. *Proc. Natl. Acad. Sci. U. S. A.* **2019**, *116*, 1495−1500.

(14) Anisimov, V. I.; Bukhvalov, D.; Rice, T. M. Electronic structure of possible nickelate analogs to the cuprates. *Phys. Rev. B* **1999**, *59*, 7901−7906.

(15) Hayward, M. A.; Green, M. A.; Rosseinsky, M. J.; Sloan, J. Sodium hydride as a powerful reducing agent for topotactic oxide deintercalation: Synthesis and characterization of the nickel(I) oxide $LaNiO_2$. *J. Am. Chem. Soc.* **1999**, *121*, 8843−8854.

(16) Ikeda, A.; Manabe, T.; Naito, M. Improved conductivity of infinite-layer $LaNiO_2$ thin films by metal organic decomposition. *Phys. C* **2013**, *495*, 134−140.

(17) Dashwood, C. D.; Miao, H.; Vale, J. G.; Ishikawa, D.; Prishchenko, D. A.; Mazurenko, V. V.; Mazurenko, V. G.; Perry, R. S.; Cao, G.; de la Torre, A.; et al. Momentum-resolved lattice dynamics of parent and electron-doped Sr_2IrO_4. *Phys. Rev. B* **2019**, *100*, No. 085131.

(18) Kurata, I.; Flores-Livas, J. A.; Sugimoto, H.; Takahashi, H.; Sagayama, H.; Yamasaki, Y.; Nomoto, T.; Arita, R.; Ishiwata, S. High-pressure synthesis of Ba_2RhO_4 a rhodate analog of the layered perovskite Sr-ruthenate. *Phys. Rev. Mater.* **2021**, *5*, No. 015001.

(19) Yvon, K.; Bezinge, A.; Tissot, P.; Fischer, P. Structure and magnetic properties of tetragonal silver(I, III) oxide, AgO. *J. Solid Stat. Chem.* **1986**, *65*, 225−230.

(20) Yang, X.; Su, H. Cuprate-like electronic properties in superlattices with $Ag^{II}F_2$ square sheet. *Sci. Rep.* **2014**, *4*, 5420.

(21) Sánchez-Movellán, I.; Moreno-Ceballos, J.; García-Fernández, P.; Aramburu, J. A.; Moreno, M. New ideas for understanding the structure and magnetism in AgF_2: Prediction of ferroelasticity. *Chem. − Eur. J.* **2021**, *27*, 13582−13590.

(22) Cheong, S. W.; Thompson, J. D.; Fisk, Z. Properties of La_2CuO_4 and related compounds. *Phys. C* **1989**, *158*, 109−126.

(23) Dai, D.; Whangbo, M. H.; Köhler, J.; Hoch, C.; Villesuzanne, A. Electronic Structure Analysis of the Difference between Cs_2AgF_4 and Rb_2MnF_4 in their magnetic properties and single-crystal structure determination of Rb_2MnF_4. *Chem. Mater.* **2006**, *18*, 3281−3286.

(24) Lee, C.; Shim, J. H.; Whangbo, M. H. Cause for the orbital ordering of Cs_2AgF_4 and its effect on thermoelectric properties. *Inorg. Chem.* **2018**, *57*, 11895−11900.

(25) Hidaka, M.; Inoue, K.; Yamada, I.; Walker, P. J. X-ray diffraction study of the crystal structures of K_2CuF_4 and $K_2Cu_xZn_{1-x}F_4$. *Physica B+C* **1983**, *121*, 343−350.

(26) McLain, S. E.; Dolgos, M. R.; Tennant, D. A.; Turner, J. F. C.; Barnes, T.; Proffen, T.; Sales, B. C.; Bewley, R. I. Magnetic behaviour of layered Ag(II) fluorides. *Nat. Mater.* **2006**, *5*, 561−565.

(27) Bersuker, I. B. *The Jahn−Teller Effect*; Cambridge University Press: Cambridge, U.K., 2009

(28) Kugel, K. I.; Khomskii, D. I. Crystal Structure and Magnetic Properties of Substances with Orbital Degeneracy. *Sov. Phys. JETP* **1973**, *37*, 725−730.

(29) Kugel, K. I.; Khomskii, D. I. The Jahn−Teller Effect and Magnetism: Transition Metal Compounds. *Sov. Phys. Usp.* **1982**, *25*, 231−256.

(30) Reinen, D.; Krause, S. Local and cooperative Jahn-Teller interactions of copper (2+) in host lattices with tetragonally compressed octahedra. Spectroscopic and structural investigation of the mixed crystals $K(Rb)_2Zn_{1-x}Cu_xF_4$. *Inorg. Chem.* **1981**, *20*, 2750−2759.

(31) Aramburu, J. A.; García-Lastra, J. M.; García-Fernández, P.; Barriuso, M. T.; Moreno, M. Cu^{2+} in layered compounds: Origin of the compressed geometry in the model system $K_2ZnF_4:Cu^{2+}$. *Inorg. Chem.* **2013**, *52*, 6923−6933.

(32) Aramburu, J. A.; García-Fernández, P.; García-Lastra, J. M.; Moreno, M. Jahn-Teller and non-Jahn-Teller systems involving CuF_6^{4-} units: Role of the internal electric field in $Ba_2ZnF_6:Cu^{2+}$ and other insulating systems. *J. Phys. Chem. C* **2017**, *121*, 5215−5224.

(33) Aramburu, J. A.; Bhowmik, A.; García-Lastra, J. M.; García-Fernández, P.; Moreno, M. Insight into compounds with Cu(H2O)6 units: New ideas for understanding Cu^{2+} in Tutton salts. *J. Phys. Chem. C* **2019**, *123*, 3088−3101.

(34) García-Fernández, P.; Moreno, M.; Aramburu, J. A. Electrostatic control of orbital ordering in noncubic crystals. *J. Phys. Chem. C* **2014**, *118*, 7554−7561.

(35) Aramburu, J. A.; García-Fernández, P.; Mathiesen, N. R.; García-Lastra, J. M.; Moreno, M. Changing the usual interpretation of the structure and ground state of Cu^{2+}-layered perovskites. *J. Phys. Chem. C* **2018**, *122*, 5071−5082.

(36) Dovesi, R.; et al. *CRYSTAL17 User's Manual*; University of Torino: Torino, 2017.

(37) Bredow, T.; Gerson, A. Effect of exchange and correlation on bulk properties of MgO, NiO and CoO. *Phys. Rev. B* **2000**, *61*, 5194−5201.

(38) Peintinger, M. F.; Oliveira, D. V.; Bredow, T. J. Consistent Gaussian basis sets of triple-zeta valence with polarization quality for solid-state calculations. *J. Comput. Chem.* **2013**, *34*, 451−459.

https://doi.org/10.1021/acs.jpcc.3c01166
J. Phys. Chem. C 2023, 127, 8332−8341

(39) CRYSTAL basis sets. https://www.crystal.unito.it/basis-sets.php. accessed January 10, 2023.
(40) García-Fernández, P.; Ghosh, S.; English, N. J.; Aramburu, J. A. Benchmark study for the application of density functional theory to the prediction of octahedral tilting in perovskites. *Phys. Rev. B* **2012**, *86*, No. 144107.
(41) Garcia-Fernandez, P.; Wojdel, J. C.; Íñiguez, J.; Junquera, J. Second-principles method for materials simulations including electron and lattice degrees of freedom. *Phys. Rev. B* **2016**, *93*, No. 195137.
(42) Guo, Y.; Langlois, J. M.; Goddard, W. A. Electronic Structure and Valence-Bond Band Structure of Cuprate Superconducting Materials. *Science* **1988**, *239*, 896−899.
(43) Weihe, H.; Güdel, H. U.; Toftlund, H. Superexchange in magnetic insulators: An interpretation of the metal-metal charge transfer energy in the Anderson theory. *Inorg. Chem.* **2000**, *39*, 1351−1362.
(44) Anderson, P. W. New approach to the theory of superexchange interactions. *Phys. Rev.* **1959**, *115*, 2−13.
(45) Anderson, P. W. Resonating Valence Bonds: A New Kind of Insulator? *Mat. Res. Bull.* **1973**, *8*, 153−160.
(46) Anderson, P. W. The resonating valence bond state in La_2CuO_4 and superconductivity. *Science* **1987**, *235*, 1196.
(47) Tuczek, F.; Solomon, E. I. Charge-Transfer States of Bridged Transition Metal Dimers: Mono- vs Binuclear Copper Azide Systems with Relevance to Oxy-Hemocyanin. *Inorg. Chem.* **1993**, *32*, 2850−2862.
(48) Brown, C. A.; Reman, J. G.; Musselman, R. L.; Solomon, E. I. Spectroscopic and Electronic Structure Studies of met-Hemerythrin Model Complexes: A Description of the Ferric-Oxo Dimer Bond. *Inorg. Chem.* **1995**, *34*, 688−717.
(49) Slater, J. C.; Koster, G. F. Simplified LCAO method for the periodic potential problem. *Phys. Rev.* **1954**, *94*, 1498−1524.
(50) Tong, J.; Kremer, R. K.; Köhler, J.; Simon, A.; Lee, C.; Kan, E.; Whangbo, M. H. The layered antiferromagnet Cs_2AgF_4: Antiferromagnetic inter-layer coupling driven by magnetic dipole-dipole interactions. *Zeit. Für Krist.* **2010**, *225*, 498−503.
(51) Griffith, J. S. *The theory of transition metal ions*; Cambridge University Press: Cambridge, U.K., 1961.
(52) Anisimov, V. I.; Zaanen, J.; Andersen, O. K. Band Theory and Mott insulators: Hubbard U instead of Stoner I. *Phys. Rev. B* **1991**, *44*, 943−954.
(53) Lee, J. H.; Fang, L.; Vlahos, E.; Ke, X.; Jung, Y. W.; Kourkoutis, L. F.; Kim, J. W.; Ryan, P. J.; Heeg, T.; Roeckerath, M.; et al. A strong ferroelectric ferromagnet created by means of spin-lattice coupling. *Nature* **2010**, *466*, 954−958.
(54) Shafer, P.; Garcia-Fernandez, P.; Aguado-Puente, P.; Damodaran, A. R.; Yadav, A. K.; Nelson, C. T.; Hsu, S. L.; Wojdel, J. C.; Iñiguez, J.; Martin, L. W.; et al. Emergent chirality in the electric polarization texture of titanate superlattices. *Proc. Natl. Acad. Sci. U. S. A.* **2018**, *115*, 915−920.
(55) Das, S.; Tang, Y. L.; Hong, Z.; Gonçalves, M. A. P.; McCarter, M. R.; Klewe, C.; Nguyen, K. X.; Gómez-Ortiz, F.; Shafer, P.; Arenholz, E.; et al. Observation of room-temperature polar skyrmions. *Nature* **2019**, *568*, 368−372.
(56) Li, S.; Ao, Z.; Zhu, J.; Ren, J.; Yi, J.; Wang, G.; Liu, W. Strain controlled ferromagnetic-antiferromagnetic transformation in Mn-Doped silicene for information transformation devices. *J. Phys. Chem. Lett.* **2017**, *8*, 1484−1488.
(57) Jaime, M.; Saul, A.; Salamon, M.; Zapf, V. S.; Harrison, N.; Durakiewicz, T.; Lashley, J. C.; Andersson, D. A.; Stanek, C. R.; Smith, J. L.; et al. Piezomagnetism and magnetoelastic memory in uranium dioxide. *Nat. Commun.* **2017**, *8*, 99.
(58) Zhang, J.; Ji, C.; Shangguan, Y.; Guo, B.; Wang, J.; Huang, F.; Lu, X.; Zhu, J. Strain-driven magnetic phase transitions from an antiferromagnetic to a ferromagnetic state in perovskite $RMnO_3$ films. *Phys. Rev. B* **2018**, *98*, No. 195133.
(59) de Jongh, L. J.; Block, R. On the exchange interactions in some 3d-Metal ionic compounds. *Physica* **1975**, *79B*, 568−593.
(60) Aramburu, J. A.; Moreno, M. Bonding of Ag^{2+} in KCl lattice. *Solid State Comm.* **1986**, *58*, 305−309.

https://doi.org/10.1021/acs.jpcc.3c01166
J. Phys. Chem. C 2023, 127, 8332−8341